


## Discrete Polynomial Optimization with Coherent Networks of Condensates and Complex Coupling Switching

Nikita Stroeve<sup>1</sup> and Natalia G. Berloff<sup>1,2,\*</sup>

<sup>1</sup>*Skolkovo Institute of Science and Technology, Bolshoy Boulevard 30, bld.1, Moscow, 121205 Russian Federation*

<sup>2</sup>*Department of Applied Mathematics and Theoretical Physics, University of Cambridge, Cambridge CB3 0WA, United Kingdom*

 (Received 8 October 2019; accepted 7 January 2021; published 5 February 2021)

Gain-dissipative platforms consisting of lasers, optical parametric oscillators and nonequilibrium condensates operating at the condensation or coherence threshold have been recently proposed as efficient analog simulators of the two-local spin Hamiltonians with continuous or discrete degrees of freedom. We show that nonequilibrium condensates *above the threshold* arranged in an interacting network may realize  $k$ -local Hamiltonians with  $k > 2$  and lead to nontrivial phase configurations. Similarly, many gain-dissipative systems that can be manipulated by optical means can bring about the ground state of the  $k$ -local Hamiltonians and solve higher-order binary optimization problems. We show how to facilitate the search for the global solution by invoking complex couplings in the system and demonstrate the efficiency of the method on the sets of complex problems. This approach offers a highly flexible new kind of computation based on gain-dissipative simulators with complex coupling switching.

DOI: [10.1103/PhysRevLett.126.050504](https://doi.org/10.1103/PhysRevLett.126.050504)

In recent years, much effort has been devoted to the development of various technological platforms that act as quantum or classical analog simulators aimed at solving certain classes of hard classical optimization problems [1–7]. It is expected that these kinds of platforms would help to efficiently solve many tasks of significant computational complexity, ranging from modeling microscopic effects and processes like the behavior of electrons in complex materials [8,9] and finding the ground state of spin glasses [10], to the applied combinatorial optimization problems such as the traveling salesman problem [11]. Large scale computational problems of this type are hard for classical von Neumann architecture, which suggests looking for fully analog or hybrid digital, analog, and quantum devices that can find a solution faster or find a better solution in a fixed time.

Nonequilibrium condensates, optical parametric oscillators, lasers, memristor crossbars, and other platforms have been considered as annealing-inspired accelerators and demonstrated successes in finding the ground state of spin Hamiltonians with continuous or discrete variables [2,6,12,13]. In particular, the coherent Ising machine has been shown to significantly outperform classical simulated annealing in terms of both accuracy and computation time to efficiently solve Max-Cut problems [2] and has shown better scalability than the quantum annealers [14]. Integrated photonic circuits that use self-phase modulation in two microring resonators were shown to act as an optical coherent Ising machine [15,16]. The lattices of exciton-polariton condensates were shown to efficiently simulate the XY Hamiltonian when operating at the condensation

threshold [12,17,18] and the extensions to minimizing Ising and  $q$ -state Potts models were also considered [19]. In all these systems, discrete Ising “spins” or continuous XY spins are encoded in the individual phase modes of the nonlinear networks. An optimization problem of interest is mapped into the quadratic unconstrained binary optimization problem (QUBO) and, therefore, into the connection matrix of the Ising network. The problem of finding the optimal solution of a QUBO problem reduces to finding the ground state of the Ising Hamiltonian, which can be related to finding the “maximum occupancy” of the collective supermode of the underlying network, as a system specific gain mechanism is continuously increased to reach the coherence threshold [12,20].

The focus of all these technological and inspired implementations of the annealer-based optimization has been on QUBO, however, there is a large class of optimization problems—the higher-order polynomial binary optimization (HOBO)—that are more naturally encoded by the  $k$ -local Hamiltonians [21,22]. HOBO is concerned with optimizing a (high degree) multivariate polynomial function in binary variables. The basic model is to maximize or minimize a  $k$ th degree polynomial function  $f(\mathbf{x})$ , where  $\mathbf{x} = (x_1, \dots, x_i, \dots, x_N)$ ,  $x_i \in \{\pm 1\}$ . The examples of HOBO are ubiquitous from the Hypergraph max-covering problem to the Frobenius and “market split” problems [22]. HOBO is a fundamental problem in integer programming and is also known as the Fourier support graph problem. Any HOBO can be mapped into the QUBO [23], however, the overhead in the number of nodes becomes prohibitive in an actual technological platform since mapping  $k$ -local Hamiltonian into a 2-local

Hamiltonian requires the introduction of an extra spin for each product of two spins, therefore, leading to extra  $N^{\lfloor k/2 \rfloor}$  physical spins, while increasing the range of the couplings which dramatically complicates the energy landscape. Therefore, it is important to consider ways to solve HOBO directly where all physical spins correspond to logical spins. In our Letter, we show that Ising machines based on nonequilibrium condensates can be used to address 4-local HOBO when operating *above* the threshold and argue that the FPGA-based CIMs, the integrated photonic circuits with multipath interferometer and coupling using a spatial light modulator (SLM) seem to be naturally suited for addressing arbitrary degree HOBO problems. Inspired by the operation of the networks of nonequilibrium condensates we propose a new optimization algorithm for solving HOBO of an arbitrary degree. Finally, we show that another physics-inspired method of turning on and off the complex coupling between the nonlinear condensates greatly enhances the search for the global minimum.

*Polynomial optimization with coherent networks.*—The optimization problem studied in this Letter is

$$\min_{\mathbf{x} \in \{-1, +1\}^N} - \sum_{\Omega} \mathbf{A}_{i_1, \dots, i_k}^k x_{i_1} \cdots x_{i_k}, \quad (1)$$

where  $\Omega = \{i_j: 1 \leq i_1 \leq i_2 \leq \dots \leq i_k \leq N\}$  and  $\mathbf{A}^k$  is the supersymmetric tensor of degree  $k$ .

To formulate the gain-dissipative platform that reaches the ground state of the HOBO by finding the “maximum occupancy” collective supermode of the underlying network of nonequilibrium condensates we consider the mean-field equations that govern such a network based on the Ginzburg-Landau equation [24,25]. This is a universal driven-dissipative equation that describes the behavior of systems in the vicinity of a symmetry-breaking instability and has been used to describe lasers, thermal convection, nematic liquid crystals, and various nonequilibrium condensates [26,27]. When derived asymptotically from a generic laser model given by Maxwell-Bloch equations it has a saturable nonlinearity and can be written as

$$i \frac{\partial \psi}{\partial t} = -\nabla^2 \psi + \tilde{U} |\psi|^2 \psi + i \left( \frac{P(\mathbf{r}, t)}{1 + b |\psi|^2} - \gamma_c \right) \psi, \quad (2)$$

where  $\psi(\mathbf{r}, t)$  is the wave function of the system,  $\tilde{U}$  is the strength of the delta-function interaction potential,  $\gamma_c$  is the rate of linear losses,  $b$  parametrizes the effective strength of nonlinear losses,  $P(\mathbf{r}, t)$  describes the gain mechanism that adds particles to the system. In writing Eq. (2) we let the Planck constant  $\hbar = 1$  and the particle mass  $m = 1/2$ . It was experimentally demonstrated [12] that when pumped at the condensation threshold, freely expanding optically imprinted polariton condensates

arranged in a lattice may achieve a steady state with condensate phases realizing the minimum of the XY Hamiltonian. In this framework, the coupling strengths between condensates depend on the system parameters, pumping intensity, shape and on the lattice geometry [28]. We shall assume that  $P(\mathbf{r}, t)$  adds particles in  $N$  spatial locations centered at  $\mathbf{r}_i$ ,  $i = 1, \dots, N$ , so that  $P(\mathbf{r}, t) = \sum_i f_i(t) p_i(\mathbf{r})$ , where  $f_i$  is the time-dependent part of the pumping at  $\mathbf{r} = \mathbf{r}_i$  and  $p_i(\mathbf{r}) \equiv p(\mathbf{r} - \mathbf{r}_i)$  is a given spatially localized pumping profile, that creates the condensate with a wave function  $\phi_i(\mathbf{r}) \equiv \phi(\mathbf{r} - \mathbf{r}_i)$  centered at  $\mathbf{r} = \mathbf{r}_i$  and normalized so that  $\int_{\Gamma} |\phi(\mathbf{r})|^2 d\mathbf{r} = 1$ , where  $\Gamma$  is the entire domain. If the distances between the neighboring condensates are larger than the width of  $p(\mathbf{r})$ , we employ the tight-binding approximation and write the wave function of the system as a linear superposition of the wave functions of individual coherent centers  $\psi(\mathbf{r}, t) \approx \sum_{i=1}^N a_i(t) \phi_i(\mathbf{r})$ , where  $a_i(t)$  is the time-dependent complex amplitude networks [19,29]. We expand the first term in the brackets of Eq. (2) in Taylor series, substitute the expressions for  $P$  and  $\psi$ , multiply by  $\phi_j^*$  for  $j = 1, \dots, N$  and eliminate the spatial degrees of freedom by integrating in the entire space to obtain  $N$  equations of the form

$$\begin{aligned} \frac{d\Psi_i}{dt} = & \Psi_i (\gamma_i - (\sigma_i + iU) |\Psi_i|^2) + \sum_{j \neq i} J_{ij} \Psi_j \\ & + \sum_{\langle j, k, l \rangle} Q_{ijkl} \Psi_j \Psi_k \Psi_l^*. \end{aligned} \quad (3)$$

In writing Eq. (3) we used the following notations:  $\Psi_i = a_i \exp(it \int_{\Gamma} \phi^* \nabla^2 \phi d\mathbf{r})$ ,  $\gamma_i = f_i \int_{\Gamma} p |\phi|^2 d\mathbf{r} - \gamma_c$ ,  $U = \tilde{U} \int_{\Gamma} |\phi|^4 d\mathbf{r}$ ,  $J_{ij} = f_j \int_{\Gamma} p_i \phi_j \phi_i^* d\mathbf{r}$  for  $j \neq i$ ,  $\sigma_i = b f_i \int_{\Gamma} p |\phi|^4 d\mathbf{r}$  and  $Q_{ijkl} = -b \sum_{m \in \{i, j, k, l\}} f_m \int_{\Gamma} p_m \phi_k \phi_l^* \phi_j \phi_i^* d\mathbf{r}$ , where  $i = j = k = l$  is excluded, which is indicated by the notation  $\langle i, j, k \rangle$  in Eq. (3) [30]. It is also possible to introduce an additive noise in Eq. (3) representing intrinsic vacuum fluctuations and classical noise [17]. The rate equations on  $\Psi_i(t)$  take the form similar to what was obtained for a polaritonic networks at the condensation threshold [17], but now involve higher-order terms represented by the supersymmetric tensor  $\mathbf{Q}$ . At the condensation threshold these terms can be neglected, however, above the threshold these terms allow to minimize the higher-order  $k$ -local Hamiltonians. To see this, we rewrite Eq. (3) in terms of the number densities  $\rho_i$  and phases  $\theta_i$  using the Madelung transformation  $\Psi_i = \sqrt{\rho_i} \exp[i\theta_i]$ :

$$\begin{aligned} \frac{1}{2} \dot{\rho}_i(t) = & (\gamma_i - \sigma_i \rho_i) \rho_i + \sum_{j \neq i} J_{ij} \sqrt{\rho_i \rho_j} \cos \theta_{ij} \\ & + \sum_{\langle j, k, l \rangle} Q_{ijkl} \sqrt{\rho_i \rho_j \rho_k \rho_l} \cos \theta_{ijkl}, \end{aligned} \quad (4)$$

$$\begin{aligned} \dot{\theta}_i(t) = & -U\rho_i - \sum_{j \neq i} J_{ij} \frac{\sqrt{\rho_j}}{\sqrt{\rho_i}} \sin \theta_{ij} \\ & - \sum_{(j,k,l)} Q_{ijkl} \frac{\sqrt{\rho_j \rho_k \rho_l}}{\sqrt{\rho_i}} \sin \theta_{ijkl}, \end{aligned} \quad (5)$$

where  $\theta_{ij} = \theta_i - \theta_j$  and  $\theta_{ijkl} = \theta_i + \theta_l - \theta_k - \theta_j$ .

Equation (5) describes the evolution of the higher-order Kuramoto oscillators that have been proposed to model higher-order interactions between neurological dynamical units [32]. The higher-order terms affect the states even in the simplest configuration of two identical oscillators pumped with  $\gamma_i = \gamma$  for which the occupancy  $\rho_0 = \rho_1 = \rho_2$  at the fixed point of Eqs. (4)–(5) reads  $\rho_0 = [\gamma + J \cos \Delta\theta + \tilde{Q} \cos(2\Delta\theta)]/\sigma$ , where  $\Delta\theta = \theta_1 - \theta_2$  and  $\tilde{Q} = \rho_0 Q$ . By choosing the minimum pumping  $\gamma$  to reach the required occupancy, we minimize the Hamiltonian  $H_{\text{two}} = -J \cos \Delta\theta - \tilde{Q} \cos(2\Delta\theta)$  while Eq. (5) describes the gradient descent to the local minimum of  $H_{\text{two}}$ . If  $\tilde{Q}$  is negligible, we have the minimization of the XY Hamiltonian, so  $\Delta\theta = 0$  or  $\pi$  if  $J > 0$  or  $J < 0$ , respectively. The same minimum is realized if  $\tilde{Q}$  is present but has the same sign as  $J$ . However, a different phase difference is realized when  $J\tilde{Q} < 0$  and  $|\tilde{Q}/J| \geq \frac{1}{4}$ , namely,  $\Delta\theta = \arccos(-J/4\tilde{Q})$ .

In the example of two oscillators the stationary state with an equal occupancy of the nodes is always reached. However, in a more general system with many oscillators, unless the oscillatory network is highly symmetric (all oscillators have an equal number of connections of the same strength with other oscillators) the system breaks into subsystems characterized by different frequencies. To guarantee the full synchronization of the network we need to choose the injection rates in such a way that all oscillators have the same occupancy. For instance, this can be achieved by introducing a feedback mechanism on the pumping rates dynamically [17].

So far we justified the appearance of tensor terms in the gain-dissipative equations using freely expanding optically imprinted condensates with geometrical couplings. As we have shown above such systems involve both quadratic and quartic terms with correlated strengths. A recently developed scheme to couple polariton condensates remotely using the spatial light modulator (SLM) overcomes this limitation [37] and allows us to generate couplings that correspond to arbitrary  $k$ -local Hamiltonians. Other gain-dissipative platforms such as the FPGA-based CIMs [3], the integrated photonic circuits with multipath interferometer and photonic SLM-based CIMs [38] seem to be naturally suited for addressing HOBO problems since DOPO FPGAs, multipath interferometers, and SLMs allow us to combine the light coming from several sources and inject into a single optical element producing required tensor terms. Many other gain-dissipative condensate systems that can be manipulated by optical means such as photon condensates in dye-polymer

solution within an ultrahigh-finesse microcavity [7] or a supersolid of dipolar excitons [39] could also be suitable as HOBO problem solvers.

*Physics-inspired optimization.*—In the view of the variety of physical gain-dissipative systems capable of following the tensor minimization we extend and simplify Eq. (3) to capture the mechanism of relaxation to the minimum of the HOBO. The minimum of HOBO for  $N$  binary variables can be found by numerical integration of  $2N$  equations

$$\frac{d\Psi_l}{dt} = \Psi_l(\gamma_l - |\Psi_l|^2) + \sum_{\tilde{\Omega}} \mathbf{A}_{i_1, \dots, i_k}^k \Psi_{i_1} \cdots \Psi_{i_k}^*, \quad (6)$$

$$\frac{d\gamma_l}{dt} = \epsilon(\rho_{\text{th}} - |\Psi_l|^2), \quad (7)$$

where  $\tilde{\Omega}$  is  $\Omega$  with excluded index  $l$  and the initial values for pumping strength are  $\gamma_l(t=0) = -\max_{1 \leq l \leq N} \sum_{\tilde{\Omega}} |\mathbf{A}_{i_1, \dots, i_k}^k|$ . Equation (7) describes the feedback mechanism that drives all  $\rho_i$  to *a priori* set values  $\rho_{\text{th}}$ ,  $\epsilon$  characterizes how fast  $\gamma_i$  adjusts to changes in  $\rho_i$ .

At the fixed point, the imaginary part of Eq. (6) gives a set of linear equations such that the  $l$ th equation involves superposition of  $\sin(\sum_{i_j \neq l, i_j < i_k} \theta_{i_j} - \theta_{i_k} - \theta_l)$  that has to be equal to zero. In general, the only way for the system to satisfy these equations is to bring all phases  $\theta_l$  to take on 0 or  $\pi$ . The total occupancy of the system at the fixed point is found from the real part of Eq. (7) and is equal to  $N\rho_{\text{th}}$ , so that  $N\rho_{\text{th}} = \sum_{l=1}^N \gamma_l + \sqrt{\rho_{\text{th}}}^{k-2} k \sum_{\tilde{\Omega}} \mathbf{A}_{i_1, \dots, i_k}^k \cos(\theta_{i_1}) \cdots \cos(\theta_{i_k})$ . If we set the process of raising the pumping from below that guarantees that  $\sum_{l=1}^N \gamma_l$  is the smallest possible injected intensity, then at the fixed point the system finds the global minimum of the  $k$ -local Hamiltonian  $H = -\sum_{\tilde{\Omega}} \mathbf{A}_{i_1, \dots, i_k}^k \cos(\theta_{i_1}) \cdots \cos(\theta_{i_k})$ , and, therefore, solves Eq. (1). We will refer to the Eqs. (6)–(7) as the tensor gain-dissipative (TGD) method.

To illustrate the behavior of the system we first consider a toy problem: the 3-local Hamiltonian

$$H_{\text{test}}(\mathbf{x}) = -8x_1x_2x_3 - 4x_1x_2x_4 - 2x_2x_3x_4 - x_1x_3x_4, \quad (8)$$

with variables  $x_i \in \{\pm 1\}$ , while Eq. (6) becomes  $\dot{\Psi}_l = \Psi_l(\gamma_l - |\Psi_l|^2) + \sum_{\tilde{\Omega}} K_{ljk} \Psi_j \Psi_k^*$ , and  $K$  is a tensor with nonzero entries 1,2,4,8. The Hamiltonian  $H_{\text{test}}$  has  $2^4$  different values, among which there are three local minima:  $H_1 = -9$ ,  $H_2 = -11$ ,  $H_3 = -13$  and the global minimum  $H_4 = -15$ , that all can be accessed during the time evolution of the system. To understand the basins of attraction for these stationary points we numerically integrate Eqs. (6)–(7) starting with initial conditions  $\Psi_i(t=0) = (1/100) \exp[i\theta_i^0]$ , where the phases  $\theta_i^0 \in [0, 2\pi)$  are uniformly distributed. Figure 1(a) depicts the statistics of the distribution of the stationary points reached and indicates that the basins of local minima combined are



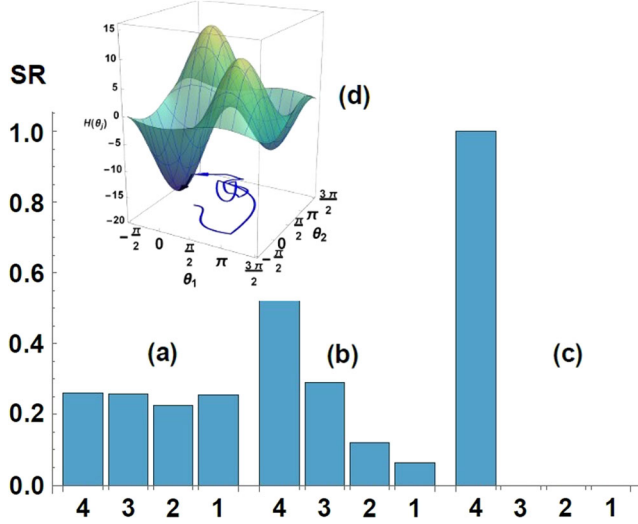


FIG. 1. Success rates for achieving minima of  $H_{\text{test}}$  given by Eq. (8) using numerical simulations of Eqs. (6)–(7) for three different controls described in the main text: fully deterministic integration without noise (a); with the white noise (b); using complex coupling control (c). Marked on the horizontal axis are minima 1,2,3,4 that correspond to  $H_1$ ,  $H_2$ ,  $H_3$ , and  $H_4$  (global minimum), respectively. The inset (d) depicts the two-dimensional projection ( $\theta_3 = \theta_4 = 0$ ) of the energy landscape for  $H_{\text{test}}$  with  $x_i = \cos \theta_i$ . The scaled and shifted total injected intensity ( $\sum \gamma_i - N\rho_{\text{th}}/3\sqrt{\rho_{\text{th}}}$  (so that it is equal to  $H_{\text{test}}$  at the steady state) found by numerical simulations of Eqs. (6)–(7) is shown by the blue trajectory in the same 2D projection.

larger than that of the global minimum. To facilitate the search for the global minimum the algorithm needs to allow for a possibility to explore the hyperspace until the lowest lying energy state is found. This can be achieved by adding a noise (typically present in the physical system as well), that shifts the trajectory from its deterministic path while allowing it to stay below any local minima. This can be ascertained by decreasing  $\epsilon$  that controls the time the system spends while raising to the condensation threshold from below. We illustrate this behavior in Fig. 1(b) that depicts the statistics of reaching local and global minima found by numerical integration of Eqs. (6)–(7) using the same initial conditions as in Fig. 1(a) but with the white noise added. Further decreasing of  $\epsilon$  allows us to improve the chances of reaching the global minima. On Fig. 1(d) we show one of such trajectories as it approaches the global minimum of  $H_{\text{test}}$  from below.

With the growth in the number of variables and concomitant growth of the system hyperspace any local noisy perturbation of the trajectory may not be sufficient to reach the global minimum basin of attraction or it would take a prohibitively long time. Recent interest in heteroclinic networks—networks that exhibit saddle states that are dynamically linked via heteroclinic connections—proposes a way to allow for fast switching between the states [40]. Motivated by these ideas we introduced

heteroclinic orbits into our model by engineering time-dependent complex couplings into the network of Eqs. (6)–(7) by replacing  $\mathbf{A}$  with  $\mathbf{A} + i\mathbf{B}(t)$ . Complex couplings often naturally appear in the governing system, e.g., due to the repulsive interactions with the non-condensed particles [41]. For instance, in polariton lattices such coupling can be turned on and off experimentally between the individual lattice elements and with strengths varying in time and space [42]. The presence of the complex part of the coupling introduces the phase lag in the system that leads to either shift of the stationary point of Eqs. (6)–(7) for small values of the complex part or destabilization of it by creating a saddle point. In the latter case, if the complex part of the coupling is turned on, the system trajectory quickly leaves the neighborhood of the previous stationary point along the fastest direction. Including this switching dynamics into the system facilitates the search for the true global minimum by allowing a fuller exploration of the phase space.

*Complex coupling switching.*—To implement the complex coupling switching on Hamiltonian given by Eq. (8) we turn two of the real coupling coefficient into the complex ones with a significant complex part as soon as the system reaches a steady state. The system trajectory leaves the basin of attraction of that state and travels to a different part of the system hypercube  $[0, 2\pi]^N$ . When the complex part of the coupling is turned off another steady state may be found. By varying the coupling elements to be switched, the duration of the switching in time and the amplitude of the imaginary coupling we allow the system to efficiently search for the global minimum. In our test example, implementing the switching of coupling coefficients  $K_{123}$  and  $K_{124}$  according to  $K_{123}(t) = 8(1 + 4i)$ ,  $K_{124}(t) = 4(1 - 10i)$ ,  $t \in [t_1, t_1 + 160] \cup [t_2, t_2 + 160] \cup [t_3, t_3 + 280]$  and keeping  $K_{123}(t) = 8$ ,  $K_{124}(t) = 4$  otherwise allows every trajectory irrespective of its initial state to arrive to the global minimum. Here  $t_1, t_2, t_3$  are times at which the system settles to a steady state after switching the complex part of the couplings off. Figure 1(c) shows convergence of all trajectories to the global minimum with 100% probability.

*Complex coupling switching for large  $N$ .*—We adapt the idea of the complex couplings switching for the large scale simulations. The elements of the dense tensors are uniformly distributed in  $[-1, 1]$ . To generate sparse tensors we take the dense tensors and randomly set 90% of all elements to zero. To implement the complex coupling switching (TGD + CC) method on large  $N$ , as soon as the system reaches the steady state we randomly choose  $N/50$  of the coupling strengths  $K_{ijk}$  (and their corresponding elements with all possible permutations of the indexes) and modify them by adding  $\chi_{ijk} = 3iK_{ijk}$ . This destabilizes the system and forces the trajectory to leave along a certain orbit. After that, we let  $\chi_{ijk} = 0$  and allow the original system to relax to a new steady state. Keeping the total

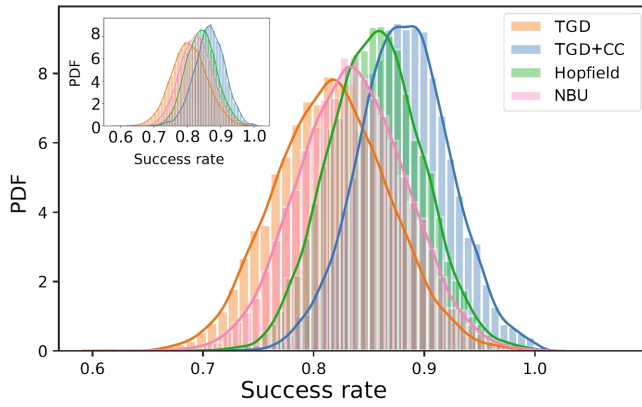


FIG. 2. The probability density function of the final solutions in comparison with the best one found (referred to as the global minimum) among 500 runs on the set of 20 dense tensors  $K_{ijk}$  in the main figure and 20 sparse tensors in the inset of the  $3^d$  rank tensors for  $N = 100$ . The running time for all algorithms was set to the same value.

injected rate  $\sum \gamma_l$  small forces the trajectories to explore the low energy states of the Hamiltonian until the true global minimum is found.

We compare the behavior of the TGD, TGD + CC with two network-based methods and show that TGD + CC outperforms these methods as Fig. 2 illustrates. The first network-based method represents the network of analog bistable units (NBU) in the presence of a double-well potential derivative that forces the network elements  $x_l$  to take on  $\pm 1$  while solving Eq. (1):

$$\frac{dx_l}{dt} = -hx_l|x_l|^{k-1}(x_l^2 - 1) + \sum_{\Omega} \mathbf{A}_{i_1, \dots, i_k}^k x_{i_1} \dots x_{i_k}, \quad (9)$$

where  $x_l(t=0)$  are randomly distributed real numbers, and  $h$  is a control parameter. In comparison with the usual  $k=2$  case [43], we balanced the degrees of polynomial between two terms on the right-hand side of Eq. (9) by introducing the  $|x_l|^{k-1}$  factor.

Another efficient solver of Eq. (1) is given by higher-order Hopfield neural networks [44]:

$$\frac{dx_l}{dt} = -x_l + \sum_{\Omega} \mathbf{A}_{i_1, \dots, i_k}^k s_{i_1} \dots s_{i_k}, \quad s_l = \tanh\left(\frac{u_l(t)}{\beta}\right), \quad (10)$$

where  $x_l$  are real continuous variables and  $\beta$  is the scaling parameter.

**Conclusions.**—We introduced an idea that the systems of gain-dissipative oscillators such as polariton condensates or lasers are capable of realizing the  $k$ -local Hamiltonians with nontrivial spin structures. We formulate a system-inspired method of computing the optimal solution of a large range of HOBO problems. Finally, we introduced the concept of computation via the mechanism of complex coupling switching—a dynamical feature that supports

switching between the local minima until the true global minimum is found.

The authors acknowledge support from Huawei.

\*Corresponding author.

N.G.Berloff@damtp.cam.ac.uk

- [1] S. Utsunomiya, K. Takata, and Y. Yamamoto, Mapping of Ising models onto injection-locked laser systems, *Opt. Express* **19**, 18091 (2011).
- [2] A. Marandi, Z. Wang, K. Takata, R.L. Byer, and Y. Yamamoto, Network of time-multiplexed optical parametric oscillators as a coherent ising machine, *Nat. Photonics* **8**, 937 (2014).
- [3] T. Inagaki, K. Inaba, R. Hamerly, K. Inoue, Y. Yamamoto, and H. Takesue, Large-scale ising spin network based on degenerate optical parametric oscillators, *Nat. Photonics* **10**, 415 (2016).
- [4] P.L. McMahon, A. Marandi, Y. Haribara, R. Hamerly, C. Langrock, S. Tamate, T. Inagaki, H. Takesue, S. Utsunomiya, K. Aihara *et al.*, A fully programmable 100-spin coherent ising machine with all-to-all connections, *Science* **354**, 614 (2016).
- [5] Y. Takeda, S. Tamate, Y. Yamamoto, H. Takesue, T. Inagaki, and S. Utsunomiya, Boltzmann sampling for an xy model using a non-degenerate optical parametric oscillator network, *Quantum Sci. Technol.* **3**, 014004 (2017).
- [6] M. Nixon, E. Ronen, A.A. Friesem, and N. Davidson, Observing Geometric Frustration with Thousands of Coupled Lasers, *Phys. Rev. Lett.* **110**, 184102 (2013).
- [7] D. Dung, C. Kurtscheid, T. Damm, J. Schmitt, F. Vewinger, M. Weitz, and J. Klaers, Variable potentials for thermalized light and coupled condensates, *Nat. Photonics* **11**, 565 (2017).
- [8] I. Buluta, S. Ashhab, and F. Nori, Natural and artificial atoms for quantum computation, *Rep. Prog. Phys.* **74**, 104401 (2011).
- [9] I.M. Georgescu, S. Ashhab, and F. Nori, Quantum simulation, *Rev. Mod. Phys.* **86**, 153 (2014).
- [10] F. Barahona, On the computational complexity of Ising spin glass models, *J. Phys. A* **15**, 3241 (1982).
- [11] *The Traveling Salesman Problem: A Guided Tour of Combinatorial Optimization*, edited by E.L. Lawler, J.K. Lenstra, A.R. Kan, D.B. Shmoys *et al.* (Wiley, New York, 1985), vol. 3.
- [12] N.G. Berloff, M. Silva, K. Kalinin, A. Askitopoulos, J.D. Töpfer, P. Cilibizzi, W. Langbein, and P.G. Lagoudakis, Realizing the classical xy hamiltonian in polariton simulators, *Nat. Mater.* **16**, 1120 (2017).
- [13] F. Cai, S. Kumar, T. Van Vaerenbergh, R. Liu, C. Li, S. Yu, Q. Xia, J.J. Yang, R. Beausoleil, W. Lu *et al.*, Harnessing intrinsic noise in memristor Hopfield neural networks for combinatorial optimization, [arXiv:1903.11194](https://arxiv.org/abs/1903.11194).
- [14] R. Hamerly, T. Inagaki, P.L. McMahon, D. Venturelli, A. Marandi, T. Onodera, E. Ng, C. Langrock, K. Inaba, T. Honjo *et al.*, Experimental investigation of performance differences between coherent ising machines and a quantum annealer, *Sci. Adv.* **5**, eaau0823 (2019).

- [15] D. Kielpinski, R. Bose, J. Pelc, T. Van Vaerenbergh, G. Mendoza, N. Tezak, and R. G. Beausoleil, Information processing with large-scale optical integrated circuits, in *2016 IEEE International Conference on Rebooting Computing (ICRC)* (IEEE, New York, 2016), pp. 1–4.
- [16] N. Tezak, T. Van Vaerenbergh, J. S. Pelc, G. J. Mendoza, D. Kielpinski, H. Mabuchi, and R. G. Beausoleil, Integrated coherent ising machines based on self-phase modulation in microring resonators, *IEEE J. Sel. Top. Quantum Electron.* **26**, 1 (2019).
- [17] K. P. Kalinin and N. G. Berloff, Networks of non-equilibrium condensates for global optimization, *New J. Phys.* **20**, 113023 (2018).
- [18] K. P. Kalinin and N. G. Berloff, Global optimization of spin hamiltonians with gain-dissipative systems, *Sci. Rep.* **8**, 17791 (2018).
- [19] K. P. Kalinin and N. G. Berloff, Simulating Ising and Potts Models and External Fields with Non-Equilibrium Condensates, *Phys. Rev. Lett.* **121**, 235302 (2018).
- [20] Z. Wang, A. Marandi, K. Wen, R. L. Byer, and Y. Yamamoto, Coherent ising machine based on degenerate optical parametric oscillators, *Phys. Rev. A* **88**, 063853 (2013).
- [21] S. He, Z. Li, and S. Zhang, Approximation algorithms for discrete polynomial optimization, *J. Oper. Res. Soc. China* **1**, 3 (2013).
- [22] B. Jiang, Z. Li, and S. Zhang, Approximation methods for complex polynomial optimization, *Comput. Optim. Applic.* **59**, 219 (2014).
- [23] G. De las Cuevas and T. S. Cubitt, Simple universal models capture all classical spin physics, *Science* **351**, 1180 (2016).
- [24] M. Wouters and I. Carusotto, Excitations in a Non-equilibrium Bose-Einstein Condensate of Exciton Polaritons, *Phys. Rev. Lett.* **99**, 140402 (2007).
- [25] J. Keeling and N. G. Berloff, Spontaneous Rotating Vortex Lattices in a Pumped Decaying Condensate, *Phys. Rev. Lett.* **100**, 250401 (2008).
- [26] I. Carusotto and C. Ciuti, Quantum fluids of light, *Rev. Mod. Phys.* **85**, 299 (2013).
- [27] J. Keeling and N. G. Berloff, Exciton–polariton condensation, *Contemp. Phys.* **52**, 131 (2011).
- [28] P. G. Lagoudakis and N. G. Berloff, A polariton graph simulator, *New J. Phys.* **19**, 125008 (2017).
- [29] A. Smerzi and A. Trombettoni, Nonlinear tight-binding approximation for Bose-Einstein condensates in a lattice, *Phys. Rev. A* **68**, 023613 (2003).
- [30] See Supplemental Material at <http://link.aps.org/supplemental/10.1103/PhysRevLett.126.050504> for the detailed derivations, assumptions used and their justifications in Sec. I A, which includes Refs. [26–28,31]; for the relationship between Eq. (5) and the higher-order Kuramoto model in Sec. II, which includes Refs. [32–36]; for the simplifying assumptions that lead to Eqs. (6)–(7) in Sec. I. B; for an illustration of the projection of the spins onto 0 or  $\pi$  as well as for a detailed description of the tensor structures used in the text in Sec. III; for the details of numerical simulations and the parameters used Sec. IV.
- [31] K. P. Kalinin, P. G. Lagoudakis, and N. G. Berloff, Matter wave coupling of spatially separated and unequally pumped polariton condensates, *Phys. Rev. B* **97**, 094512 (2018).
- [32] P. S. Skardal and A. Arenas, Higher order interactions in complex networks of phase oscillators promote abrupt synchronization switching, *Commun. Phys.* **3**, 218 (2020).
- [33] J. A. Acebrón, L. L. Bonilla, C. J. P. Vicente, F. Ritort, and R. Spigler, The Kuramoto model: A simple paradigm for synchronization phenomena, *Rev. Mod. Phys.* **77**, 137 (2005).
- [34] I. León and D. Pazó, Phase reduction beyond the first order: The case of the mean-field complex Ginzburg-Landau equation, *Phys. Rev. E* **100**, 012211 (2019).
- [35] A. Pizzi, F. Dolcini, and K. Le Hur, Quench-induced dynamical phase transitions and  $\pi$ -synchronization in the Bose-Hubbard model, *Phys. Rev. B* **99**, 094301 (2019).
- [36] D. Witthaut and M. Timme, Kuramoto dynamics in Hamiltonian systems, *Phys. Rev. E* **90**, 032917 (2014).
- [37] K. P. Kalinin, A. Amo, J. Bloch, and N. G. Berloff, Polaritonic XY-Ising machine, *Nanophotonics* **9**, 20200162 (2020).
- [38] D. Pierangeli, G. Marcucci, and C. Conti, Large-Scale Photonic Ising Machine by Spatial Light Modulation, *Phys. Rev. Lett.* **122**, 213902 (2019).
- [39] S. Andreev, Fragmented-condensate solid of dipolar excitons, *Phys. Rev. B* **95**, 184519 (2017).
- [40] F. S. Neves and M. Timme, Computation by Switching in Complex Networks of States, *Phys. Rev. Lett.* **109**, 018701 (2012).
- [41] K. P. Kalinin and N. G. Berloff, Polaritonic network as a paradigm for dynamics of coupled oscillators, *Phys. Rev. B* **100**, 245306 (2019).
- [42] S. Alyatkin, J. D. Töpfer, A. Askitopoulos, H. Sigurdsson, and P. G. Lagoudakis, Optical Control of Synchronous Phases in a Programmable Polariton Cell, *Phys. Rev. Lett.* **124**, 207402 (2020).
- [43] T. Leleu, Y. Yamamoto, P. L. McMahon, and K. Aihara, Destabilization of Local Minima in Analog Spin Systems by Correction of Amplitude Heterogeneity, *Phys. Rev. Lett.* **122**, 040607 (2019).
- [44] G. Joya, M. Atencia, and F. Sandoval, Hopfield neural networks for optimization: Study of the different dynamics, *Neurocomputing; Variable Star Bulletin* **43**, 219 (2002).